Stress generation, relaxation and size control in confined tumor growth

H. Yan,[1] D. Ramirez-Guerrero,[1,2] J. Lowengrub*,[1,2,3,4] and M. Wu†[5]

[1]*Mathematics, University of California, Irvine, Irvine, California, Irvine, 92697, California , USA*
[2]*Center for Multiscale Cell Fate Studies, University of California, Irvine, Irvine, California, Irvine, 92697, California , USA*
[3]*Biomedical Engineering, University of California, Irvine, Irvine, California, Irvine, 92697, California , USA*
[4]*Center for Complex Biological Systems, University of California, Irvine, Irvine, California, Irvine, 92697, California , USA*
[5]*Mathematical Sciences, Worcester Polytechnic Institute, Worcester, 01605, Massachusetts , USA*

(Dated: September 6, 2019)

Experiments on tumor spheroids have shown that compressive stress from their environment can reversibly decrease tumor expansion rates and final sizes. Stress release experiments show that nonuniform anisotropic elastic stresses can be distributed throughout. The elastic stresses are maintained by structural proteins and adhesive molecules, and can be actively relaxed by a variety of biophysical processes. In this letter, we present a new continuum model to investigate how the instantaneous elastic moduli and active stress relaxation, in conjunction with mechanical feedback machinery within cells, regulate the sizes of and stress distributions within growing tumors in the presence of external physical confinement and gradients of growth-promoting chemical fields. We introduce an adaptive reference map that relates the current position with the reference position but adapts to the current position in the Eulerian frame (lab coordinates) via relaxation. This type of stress relaxation is similar to but simpler than the classical Maxwell model of viscoelasticity. By fitting the model to experimental data from two independent studies of tumor spheroid growth, treating the tumors as incompressible, neo-Hookean elastic materials, we find that the rates of stress relaxation of tumor tissues can be comparable to volumetric growth rates. Our study provides insight on how the biophysical properties of the tumor and host microenvironment, mechanical feedback control and diffusion-limited differential growth act in concert to regulate spatial patterns of stress and growth. When the tumor is stiffer than the host, our model predicts tumors are more able to change their size and mechanical state autonomously, which may help to explain why increased tumor stiffness is an established hallmark of malignant tumors.

PACS numbers: 46.15.Cc,62.20.mt,68.55.at,87.19.1x,87.19.R-

Introduction The importance of mechanical forces in regulating cell behaviors during normal development and homeostasis [1, 2], and in disease progression such as cancer [3–5], is now widely recognized. In addition to driving cell movement and deformation, biophysical forces act via mechanotransduction to regulate cell fates, division, and death rates [6–9]. Nevertheless, the effects of tissue properties and mechanical stresses on cancer progression and treatment outcomes are still not well understood. *In vitro* experiments on avascular tumor spheroids have shown that changes in their mechanical environment can result in different tumor expansion rates, stress distributions and final sizes [10–13]. Further, it was recently observed that the material properties of tissues and external mechanical compression may play distinct roles in tumor growth [14]. In addition to mechanical compression from the exterior environment, stresses within growing tumors can be generated by nutrient-driven differential growth of cells as well as active contractility of cells [15]. The release of these stresses, by cutting, slicing, or punch protocols [14, 16], can cause finite deformations at rates faster than those of a typical cell cycle and these deformations can be used to estimate the residual elastic stress. The elastic stresses are maintained by structural proteins and adhesive molecules [17], and can be actively relaxed due to processes such as turnover/reassembly of structural and adhesion molecules, cell re-arrangements, and oriented cell divisions [1] at timescales spanning from minutes to hours [17, 18].

In this letter, we present a new continuum model in the laboratory (Eulerian) frame to investigate how a tumor spheroid modulates its size and stress distribution via internal stress relaxation in the context of external physical confinement and limited nutrient diffusion in conjunction with mechanical feedback machinery within cells. This approach facilitates the coupling between nonlinear elastic stresses, which are traditionally described using material coordinates (Lagrangian frame), and reaction-diffusion equations that model tissue growth and the dynamics of cell substrates (e.g, oxygen and nutrients), which are traditionally described in the Eulerian frame. We fit the model to experimental data from two independent studies of tumor spheroid growth and perform parametric studies around the fitted parameter regime.

The model *Tissue elasticity in an Eulerian frame–* We formulate the elastic stresses using Eulerian coordinates. Let $y(r,t)$ denote the reference map, which relates the current and reference positions in the tissue [19, 20]. Then, in radial coordinates y satisfies $\partial_t y(r,t) + v(r,t)\partial_r y(r,t) = 0$, where v is the cell velocity and $y(r,0) = r$, assuming the initial state is unstressed. Treating the tumor spheroid as an incompressible, neo-Hookean elastic material the nondimensional elastic

*lowengrb@math.uci.edu
†mwu2@wpi.edu

stresses can be written as

$$\sigma_{rr} = (\frac{y}{r}/\frac{\partial y}{\partial r})^{4/3},\ \sigma_{\theta\theta} = (\frac{\partial y}{\partial r}/\frac{y}{r})^{2/3},\ \sigma_{\phi\phi} = \sigma_{\theta\theta}, \quad (1)$$

where we have nondimensionalized the stress using the shear modulus of the tumor tissue. This approach can also be used for more general constitutive laws [21]. The total stress is $\boldsymbol{\sigma}^{tot} = \boldsymbol{\sigma} - p\mathbf{I}$ where p is the pressure. Further, time and space are nondimensionalized using the characteristic cell-cycle time scale of $\tau = 1$ day and a length scale of $l = 1\mu m$. See Secs. S1 and S2 in the Supplemental Material [22] for the full, nonsymmetric, dimensional model and nondimensionalization.

Adaptive reference map and stress relaxation– We describe the relaxation of the elastic stresses in Eq. (1) by introducing the relaxation rate β that reflects how rapidly the reference coordinates adapt to the current coordinates:

$$\frac{\partial y}{\partial t} + v \cdot \frac{\partial y}{\partial r} = \beta(r - y). \quad (2)$$

Notice the dynamics of the displacement field $u = x - y$ becomes $\partial_t u = v - \beta u$, which decays with a rate of β. Combining Eqs. (1) and (2) yields a Maxwell-like stress relaxation. See Sec. S1.4 in [22] for more details. This is similar in spirit to the approach used in [23] to model viscoelasticity in the context of a model of the cell cytoskeleton.

Force balance inside the tumor– We model the tissue as an overdamped, incompressible, nonlinear elastic material so that at any point in the tissue the velocity is proportional to the force. Using radial symmetry, the nondimensional system is:

$$\alpha v = -\frac{\partial p}{\partial r} + \frac{\partial \sigma_{rr}}{\partial r} + \frac{2}{r}(\sigma_{rr} - \sigma_{\theta\theta}), \quad (3)$$

where α is the nondimensional friction (drag) coefficient and v is the radial velocity. We denote the total radial and circumferential stresses by $\sigma_{rr}^{tot} = \sigma_{rr} - p$ and $\sigma_{\theta\theta}^{tot} = \sigma_{\theta\theta} - p$, respectively.

External compression– At the spheroid boundary $r = R$, we have the force balance relation

$$\sigma_{rr}^{tot}(R,t) = \sigma_{rr}(R,t) - p(R,t) = -F_{ext}, \quad (4)$$

where $-F_{ext}$ represents the result of external physical confinement from a surrounding solid material, externally applied hydrostatic pressure, or surface tension. Assuming that the spherical tissue grows within an incompressible neo-Hookean material, similar to the experimental set-up in [10], the external compression at the tumor boundary can be written as a function of the initial and current radius, R_0 and $R(t)$, respectively (see Sec. S3.1 in [22]):

$$F_{ext} = \frac{c_H}{2}\left(5 - \frac{R_0(R_0^3 + 4R(t)^3)}{R(t)^4}\right), \quad (5)$$

where c_H is the shear modulus of the surrounding material relative to that of the tumor tissue. Alternatively, if a hydrostatic pressure $\bar{p}$ is applied, as in [12, 13], then $F_{ext} = \bar{p}$.

Growth and chemomechanical feedback– We assume the nondimensional local volumetric growth rate of the tissue is given by $\lambda_{net}(r,t) = \lambda(r,t)c - \lambda_A(r,t)$, where $\lambda(r,t)$ is the rate of volume increase (e.g., cell proliferation), c is the concentration of a growth promoting biochemical factor that represents the net effect of diffusible substances (e.g., oxygen, glucose) on growth, and $\lambda_A(r,t)$ is the rate of volume loss (e.g., due to cell compression and death). Since the tumor spheroid is incompressible, the radial velocity $v(r,t)$ is:

$$v(r,t) = \frac{1}{r^2}\int_0^r (\lambda(\eta,t)c - \lambda_A(\eta,t))\eta^2 d\eta, \quad (6)$$

and the tumor radius evolves via $dR(t)/dt = v(R,t)$. As the tumor size changes, c can be modeled as

$$c(r,t) = (R(t)\sinh(\frac{r}{L}))/(r\sinh(\frac{R(t)}{L})), \quad (7)$$

assuming the substrate diffuses in from the tissue boundary, with $c(R(t),t) = 1$, and is uptaken by tumor cells. Here, L is the nondimensional diffusion length. See Sec. S3 in [22] for details. Because compressive stresses can reduce cell sizes and rates of cell proliferation (e.g., [12, 13]) and can increase rates of cell death (e.g., [10, 11]), we model the rates of volume increase and loss, respectively, as Hill-type equations:

$$\lambda(r,t) = \frac{\lambda_0}{1 + \gamma_\lambda(\sigma_{\theta\theta}^{tot})^n \cdot 1_{\{\sigma_{\theta\theta}^{tot}<0\}}}, \quad (8)$$

$$\lambda_A(r,t) = \lambda_{A,0} + \Delta_A \frac{\gamma_A(\sigma_{\theta\theta}^{tot})^m \cdot 1_{\{\sigma_{\theta\theta}^{tot}<0\}}}{1 + \gamma_A(\sigma_{\theta\theta}^{tot})^m \cdot 1_{\{\sigma_{\theta\theta}^{tot}<0\}}}, \quad (9)$$

where λ_0 and $\lambda_{A,0}$ are base rates, γ_λ and γ_A are feedback gains, Δ_A is the maximum change of the rate of volume loss, n and m are positive even integers, and 1_χ denotes the characteristic function of the set χ. We also assume that circumferential stresses $\sigma_{\theta\theta}^{tot}$ dominate the mechanical state of the cells because the circumferential stress represents stresses from two principle directions while radial stress σ_{rr}^{tot} accounts for only one. For simplicity, we assume that tensile stresses do not influence these rates and that any delays in cell responses to the stresses are negligible on typical cell-cycle timescales.

Results *A tumor spheroid growing with stress relaxation–* We first simulate numerically (see Sec. S3 in [22] for the algorithm), the unconfined (free) growth of an initially unstressed tumor spheroid ($F_{ext} = 0$). As seen in Fig. 1A the tumor radius increases over time and approaches a steady-state, which is independent of the initial size or initial stress state (Fig. S11 in [22]). Because of diffusion-limited nutrient transport, the net volume rate of change $\lambda_{net}(r,t) = \lambda(r,t)c(r,t) - \lambda_A(r,t)$ is spatially varying (Fig. 1B). At early times when the tumor is small, the volume increases all throughout the tumor spheroid as nutrients are readily available. At later times, volume gain (growth) dominates at the spheroid boundary and volume loss (cell death) dominates at the spheroid center (Fig. 1B) where nutrient levels are low. Correspondingly, cells move outward at early times but at late times,

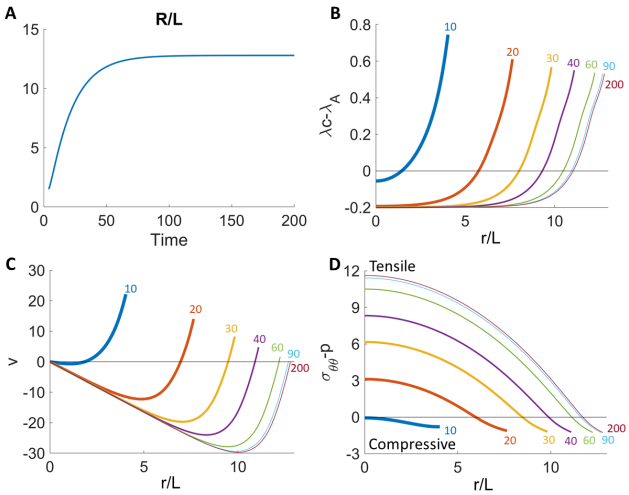

FIG. 1: Time evolution of a freely growing tumor without external compression (A). The spatial distribution of the net volumetric growth rate at different times (B). The cell velocity (C). The spatial distribution of circumferential stresses at different times (D). See text for details.

as in previous models (e.g., [12, 24, 25]), cells divide at the boundary and move inward to compensate for the loss of volume at the center (Fig. 1C), which may explain the presence of long-lasting apoptotic markers in the core of the tumor spheroids. Correspondingly, the total circumferential stresses $\sigma_{\theta\theta}^{tot}$ are compressive throughout the tumor spheroid at early times while at later times the stresses are compressive near the tumor edge and tensile in the center (Fig. 1D). See Fig. S8B for σ_{rr}^{tot} and p. Further, the stresses equilibrate as soon as the tumor radius reaches equilibrium. When the tumor reaches its equilibrium size $R(t) = R_\infty$, one can derive $y_{,r}(R_\infty) = \beta/\left(\beta + \lambda(R_\infty) - \lambda_A(R_\infty)\right)$. This shows that (i) $\beta = 0$ (no relaxation) leads to a singularity in the elastic strain and (ii) increasing β restores the proportionality between $y(r,t)$ and r and thus decreases the elastic energy (Fig. S17) and stress anisotropy (Fig. S16), which are both 0 when $y(r,t) = r$. Similar considerations hold at the tumor center.

Inhibition of growth through external confinement– In [10], it was shown that the growth capacity of tumor spheroids (human colon adenocarcinoma, LS174T) in agarose gels decreases as the concentration of agarose is increased (Figs. 2A and S2A, symbols); the stiffness of the gels is positively correlated with the agarose concentration. However, tumors suspended in gels with lower growth rates regain their free-growth capacity once the gels are removed (Fig. 2B, symbols). We use our model to fit the experimental data from tumors grown in free suspension (0% gel) and 0.7% and 1.0% agarose gels using the same set of the tumor-associated parameters (which characterize the base rates and chemomechanical responses of LS174T) but different shear moduli of the gel (e.g., $c_H = 0$ for 0% and $c_H > 0$ for the 0.7% and 1.0% gels). Following [10], we assume that cell division is insensitive to the elastic stresses ($\gamma_\lambda = 0$) but that stresses increase cell death and compression ($\gamma_A,\ \Delta_A > 0$). Then, using the same tumor-associated parameters, we fit the other gel concentrations (Fig. S2A in [22]) by changing only c_H. See Sec. S4 in [22] for details on the fitting process.

We find that the nondimensional relaxation rate $\beta \sim 1$, which suggests that a fully nonlinear elastic model is needed to describe tumor biomechanics, rather than a fluid model or a linear elastic model. Such reduced models arise as limits of our model where $\beta >> |\lambda_{net}|$. See Sec. S2 in [22] for limiting cases in different parameter regimes. The results are presented in Fig. 2 (and Figs. S2, S3 in [22]). There is good quantitative agreement between the model (curves) and experiments (symbols) for the dynamics of the tumor spheroid radii (Fig. 2A) where the bands show the results using parameters for which the results are within 10% of the best fit, which corresponds to $\beta = 0.4$ and $c_H^{1.0\%} = 1.8$ and $c_H^{0.7\%} = 0.6$ (see Sec. 4 in [22] for all the fitted parameters). Fits to other gel concentrations are shown in Fig. S2A in [22]. For the case of the 1.0% gel at equilibrium, we predict the circumferential stress ($\sigma_{\theta\theta}^{tot}$) in the tumor at equilibrium is compressive and quasi-uniform (Fig. 2C). We find that the average elastic energy in the tumor spheroid $\frac{3}{4R_\infty^3}\int_0^{R_\infty} W(y, r, \frac{\partial y}{\partial r}) r^2 dr$ decreases even though c_H increases (Fig. S3 in [22]), which shows that stress and stiffness are not always positively correlated. Not that in [14], it was found that the stress and stiffness of the tumor itself are not always positively correlated. Our results suggest that as c_H increases, the stresses in the tumor become mainly hydrostatic. When $c_H >> 1$, it can be seen analytically that the leading-order stress distribution is uniform and is given by the compression at the boundary. As the agarose concentration of the gel is decreased, c_H decreases and the stresses are less compressive and less uniform (Fig. 2C, solid curves). In the freely growing case, the stress becomes tensile in the tumor interior and is compressive only at the spheroid boundary similar to that observed in Fig. 1D. In contrast, the stresses in the gel (dotted curves) are tensile, as the growth of the tumor stretches the surrounding gels circumferentially, with the maximum stress occurring at the spheroid boundary. Increasing the gel concentration, reduces the magnitude of the circumferential stresses outside the tumor because even though c_H increases, the smaller tumors displace the gel less. At equilibrium, there is a net volume loss in the tumor center, which is balanced by volume gain at the boundary (Fig. 2D, solid curves).

To examine the effect of feedback, we also fit the data without considering feedback from the elastic stress ($\gamma_A = 0$). In this case, the predicted radii (dashed curves in Fig. 2A) also provide a good fit of the data, but the stress distributions and net volume growth rates are more heterogeneous when considering growth regulated by nutrient level alone (Figs. 2C and 2D, dashed). Further, using the corrected Akaike information criterion (AICc) [28] suggests the model with feedback provides a better fit to the experiment (not shown). Moreover, the gel-removal experiments cannot be reproduced without considering feedback from elastic stress.

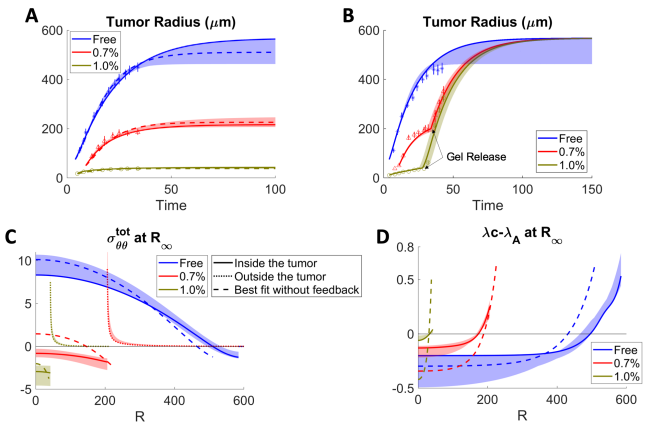

FIG. 2: Fitting the model to data from [10] of tumor spheroids grown in free suspension (blue) and 0.7% (red) and 1.0% (brown) agarose gels with (solid) and without (dashed) feedback from the elastic stress (A) and when stresses are released by removing the gels (B). Bands show the results within 10% of the best fit with feedback and in addition in (B) the gel is removed in a narrow interval around the times reported in [10]. (C) and (D): The distributions of stresses and net volume growth rates from the model. See the text for details.

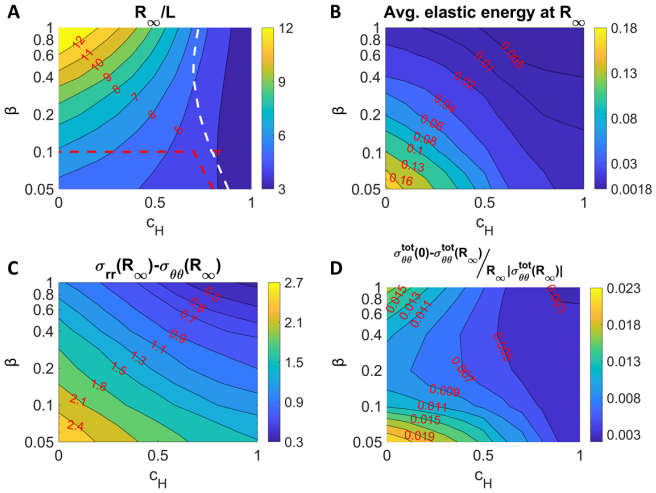

FIG. 3: Contour plot of steady-state tumor radius (A), average elastic energy in the tumor at steady-state (B), stress anisotropy at tumor boundary (C), and averaged stress gradient in the tumor, (D), as a function of β and c_H. The dashed white line shows the $\sigma_{\theta\theta}^{tot}(0) = 0$ contour. The dashed red line shows the region where the dynamics of the radius are non-monotone (see Fig. S12C). See the main text for more explanation.

To model the gel-removal experiments (Fig. 2B), we set $c_H = 0$ in all the gel cases and use the common set of fitted tumor-associated parameters (see Sec. 4 in [22] for details). Again there is good quantitative agreement between the numerics and experiments, which both tend to recover the growth of the unconstrained spheroid.

Tumor sizes and stress patterns at equilibrium– Next, we perform a parametric study to investigate how the internal stress relaxation and external spatial confinement influence the sizes of tumor spheroids, their stress distributions and anisotropies. At equilibrium, tumor sizes decrease with c_H and increase with β due to external loading and internal relaxation, respectively (Fig. 3A). The white dashed curve marks the boundary between tumor spheroids with tensile (to the left) and compressive (to the right) stresses at the spheroid center. When both c_H and β increase, the stress is less elastic and more hydrostatic (Fig. 3B) and less anisotropic (Fig. 3C). In addition, the stress distributions along the tumor radii (Fig. 3D) become more uniform and less sensitive to changes in β when c_H increases, since the stress are dominated by compression from the external loading. When β and c_H lie within the region marked by the dashed red curve in Fig. 3A, the tumors are small but their stress distributions can be heterogeneous (Fig. 3D). Interestingly, the corresponding dynamics of the spheroid radii are non-monotone as the stress equilibrates slowly towards the steady-state (Fig. S12C in [22]); we have not seen this in published data, however. Following [29], we anticipate this could lead to a break in radial symmetry. See Figs. S8-10, S13-S17 in [22] for details of the radii, stresses and elastic energy and energy density distributions.

Discussion We have developed and applied a new model of stress relaxation in the context of solid tumor growth using an Eulerian framework. The resulting system is similar to but simpler than of the classical Maxwell model of viscoelasticity. We considered the influence of elastic stress on rates of net volume changes (e.g., growth, death, compression of cells) during growth and found good agreement with experimental data from [10, 12, 13] where the volumetric growth rates of tumor spheroids adjust as the level of external confinement [10] or hydrostatic compression [12, 13] (presented in Sec. S4 in SM [22]) varies. By fitting spheroid data from these two independent studies using different tumor cell lines, we find the relaxation rate $\beta \sim 1$ per day, which is comparable to the volumetric growth rate of the tumor. Our model predicts that feedback from elastic stresses result in a more uniform spatial pattern of growth rates, which is analogous to the spatial patterning of cell proliferation observed during development of the *Drosophila* wing disc [30–32] where feedback from elastic stresses was also found to be important for this pattern of growth. We found that when the compression from external confinement is non-negligible compared to the internal compression generated by differential growth, the tumor spheroid sizes and the stress distributions are not sensitive to changes in the material properties of the spheroids. Further, the total stress is nearly uniform and is dominated by hydrostatic pressure.

We can also gain insight on tumor growth *in vivo*. When a tumor increases its instantaneous elasticity relative to the external confinement (e.g., decreasing c_H), such tumors are more able to change their size and mechanical state autonomously. This may explain why increased tumor stiffness is an established hallmark in tumor malignancy [18, 33]. On one hand, when c_H is small, the tumor size can be increased

by increasing the stress relaxation rate β. On the other hand when β is small, the tumors have large elastic energy and anisotropy and the model predicts that the dynamics of the tumor can be non-monotone, although we have not seen this observed in published data. However, we anticipate that such tumors may be subject to morphological instability, increasing local invasiveness. In summary, we suggest that when the tumor stiffness dominates over the surrounding compressive stresses, then active relaxation – an effect from lumping the turnover and deposition of intracellular cytoskeleton structures, intercellular adhesion complexes, and extracellular matrices– can be used to leverage against local invasiveness and bulk expansion during tumor progression.

Acknowledgments.- J.L., H.Y. and D.R-G. acknowledge partial funding from the National Science Foundation-Division of Mathematical Sciences (NSF-DMS) grants DMS-1714973 and DMS-1763272/Simons Foundation (594598, QN) for the Center for Multiscale Cell Fate Research at UC Irvine. JL additionally acknowledges partial funding from the National Institutes of Health (NIH) grant 1U54CA217378-01A1 for a National Center in Cancer Systems Biology at the UC Irvine (also provided support to H.Y.), and from NIH grant P30CA062203 for the Chao Family Comprehensive Cancer Center at UC Irvine.

[1] L. LeGoff and T. Lecuit, Cold Spring Harb. Perspect. Biol. **8**, a019232 (2016).
[2] F. Julicher and S. Eaton, Sem. Cell. Dev. Biol. **67**, 103 (2017).
[3] R. Jain, J. Martin, and T. Styianopoulos, Annu. Rev. Biomed. Eng. **16**, 321 (2014).
[4] H. Kim, T. Jackson, and L. Davidson, Sem. Cell. Dev. Biol. **67**, 113 (2017).
[5] J. Northcott, I. Dean, J. Mouw, and V. Weaver, Frontiers in Cell and Dev. Biol. **6**, 17 (2018).
[6] M. H. Hsieh and H. T. Nguyen, International review of cytology **245**, 45 (2005).
[7] K. C. Clause, L. J. Liu, and K. Tobita, Cell communication & adhesion **17**, 48 (2010).
[8] A. Kumar, J. Placone, and A. Engler, Development **144**, 4261 (2017).
[9] L. Schwartz, J. da Veiga Moreira, and M. Jolicoeur, Journal of cellular and molecular medicine **22**, 738 (2018).
[10] G. Helmlinger, P. A. Netti, H. C. Lichtenbeld, R. J. Melder, and R. K. Jain, Nature biotechnology **15**, 778 (1997).
[11] G. Cheng, J. Tse, R. K. Jain, and L. L. Munn, PLoS one **4**, e4632 (2009).
[12] F. Montel, M. Delarue, J. Elgeti, L. Malaquin, M. Basan, T. Risler, B. Cabane, D. Vignjevic, J. Prost, G. Cappello, *et al.*, Physical review letters **107**, 188102 (2011).
[13] M. Delarue, F. Montel, D. Vignjevic, J. Prost, J.-F. Joanny, and G. Cappello, Biophysical journal **107**, 1821 (2014).
[14] H. T. Nia, G. Seano, M. Datta, D. Jones, N. Rahbari, J. Incio, V. P. Chuahan, K. Jung, J. D. Martin, V. Askoxylakis, T. P. Padera, D. Fukumura, Y. Boucher, F. J. Hornicek, A. J. Grodzinsky, J. W. Baish, L. L. Munn, and R. K. Jain, Nature biomedical engineering **1**, 0004 (2016).
[15] W. Lee, N. Kalashnikov, S. Mok, R. Haloui, E. Kuzmin, A. Putnam, S. Takayama, M. Park, L. McCaffrey, R. Zhao, R. Leask, and C. Moraes, Nature Comm. **10**, 144 (2019).
[16] H. T. Nia, M. Datta, G. Seano, P. Huang, L. L. Munn, and R. K. Jain, Nature protocols **13**, 1091 (2018).
[17] K. Doubrovinski, M. Swan, O. Polyakov, and E. F. Wieschaus, Proceedings of the National Academy of Sciences **114**, 1051 (2017).
[18] T. R. Cox and J. T. Erler, Disease models & mechanisms , dmm (2011).
[19] H.-G. Cottet, E. Maitre, and T. Milcent, ESAIM **42**, 471 (2008).
[20] K. Kamrin, C. Rycroft, and J. Nave, J. Mech. Phys. Sol. **60**, 1952 (2012).
[21] Y. Fung, *Motion, Flow, Stress and Growth* (Springer-Verlag, 1990).
[22] *Supplementary Material*.
[23] C. Copos and R. Guy, ANZIAM J. **59**, 472 (2018).
[24] A. Jones, H. Byrne, J. Gibson, and J. Dold, Journal of mathematical biology **40**, 473 (2000).
[25] R. P. Araujo and D. S. McElwain, SIAM Journal on Applied Mathematics **66**, 447 (2005).
[26] C. Collins, J. Shen, and S. Wise, Comm. Comput. Phys. **13**, 929 (2013).
[27] D. Ambrosi and F. Mollica, International journal of engineering science **40**, 1297 (2002).
[28] K. Burnham and D. Anderson, *Model Selection and Multimodel Inference: A practical information-theoretic approach (2nd ed.)* (Springer-Verlag, 2002).
[29] A. Goriely and M. B. Amar, Physical review letters **94**, 198103 (2005).
[30] B. I. Shraiman, Proceedings of the National Academy of Sciences **102**, 3318 (2005).
[31] Y. Pan, I. Heemskerk, C. Ibar, B. I. Shraiman, and K. D. Irvine, Proceedings of the National Academy of Sciences **113**, E6974 (2016).
[32] K. D. Irvine and B. I. Shraiman, Development **144**, 4238 (2017).
[33] P. Lu, V. M. Weaver, and Z. Werb, J Cell Biol **196**, 395 (2012).